ROYAL SOCIETY
OF CHEMISTRY

PAPER

Check for updates

The complex interplay of chemo- and bio-catalysis for one-pot oxidation cascades – indole oxidation in focus

Alex Stenner, [ID] *[a] Richard J. Lewis, [ID] *[a] Johnathan Pask,[a] David J. Morgan, [ID] [a,b]
Thomas E. Davies[a] and Graham J. Hutchings [ID] *[a]

The combination of chloroperoxidase (CPO), derived from the marine fungus *Caldariomyces fumago*, in combination with supported AuPd nanoalloys, has been demonstrated as a highly efficient one-pot system for the selective oxidation of indole to 2-oxindole. Peroxy-enzymatic oxygen transfer is driven *via* chemo-catalytic *in situ* H_2O_2 generation from H_2 and O_2 over AuPd surfaces, with the continuous supply of the oxidant at low-concentration essential in maintaining enzymatic activity. Indeed, coupling CPO and an optimised 1% Au_1Pd_1/TiO_2 formulation achieved 33 000 TTN for indole oxidation, which is among the highest reported when compared to alternative systems utilizing *in situ* generated H_2O_2, including electrochemical and co-enzymatic approaches. Exceptional tandem performance has been achieved upon adopting a holistic approach toward design and optimisation of the system, thus deconvoluting the complex array of parameters governing chemo- and bio-catalytic performance under operational conditions; including metal nanoparticle speciation, morphology, electronic structure, and leaching, in addition to enzyme deactivation and *in situ* physisorption. We consider such an approach to offer a case study and guide to the community, facilitating efficient optimisation of complex chemo-enzymatic systems for potential industrial applications.

Green foundation

1. The selective oxidation of indole to 2-oxindole currently relies on the application of stoichiometric oxidants, resulting in the generation of large quantities of hazardous by-products and poor atom efficiency. Further complexity arises from the need to apply protecting/de-protecting protocols to control regioselectivity. Our chemo-enzymatic approach for such chemical transformations offers significantly improved process efficiency and product selectivity under comparatively mild operating conditions.

2. Chloroperoxidase (CPO) offers exceptional performance towards selective indole oxidation, however its synthetic potential is limited by its susceptibility to peroxidative inactivation. Our work demonstrates that exceptional enzymatic performance can be achieved upon generating H_2O_2 *in situ* from H_2 and O_2 over supported AuPd nanoparticles, which facilitates the continuous supply of low concentrations of H_2O_2 required to maintain CPO activity, while avoiding the limitations of other approaches.

3. Further catalyst design is required to enhance AuPd nanoalloy stability under operating conditions, facilitating enhanced chemo-enzymatic cascade efficacy over extended lifetimes.

Introduction

The selective oxidation of indole to 2-oxindole is a highly valuable chemical transformation for the production of pharmaceutical products, with numerous cancer, Parkinson's disease, and pulmonary fibrosis therapeutics bearing this oxygenated

[a]*Max Planck–Cardiff Centre on the Fundamentals of Heterogeneous Catalysis FUNCAT, Cardiff Catalysis Institute, School of Chemistry, Cardiff University, CF24 4HQ, UK. E-mail: StennerAJ@Cardiff.ac.uk, LewisR27@Cardiff.ac.uk, Hutch@Cardiff.ac.uk*
[b]*HarwellXPS, Research Complex at Harwell (RCaH), Didcot, OX11 OFA, UK*

heterocyclic moiety.[1–5] Conventional chemical indole oxidation approaches require stoichiometric consumption of toxic reagents (*e.g.* trichloroisocyanuric acid, *N*-bromosuccinimide, dimethyldioxirane, *meta*-chloroperoxybenzoic acid), resulting in the formation of hazardous by-products and poor atom economy.[6–9] Protecting groups and substituted indole rings are often necessary to control the regioselectivity for oxidation at the C-2 position under such protocols, owing to the competing activity at the electron-rich C-3 and N-centres, which hampers the overall process efficiency.[10]

The application of chloroperoxidase (CPO), derived from marine fungus *Caldariomyces fumago*, offers a highly attractive

enzymatic alternative, avoiding many of the drawbacks associated with conventional chemical approaches. The heme-thiolate enzyme requires only H_2O_2 to maintain biocatalytic activity, which mitigates stoichiometric consumption of ancillary flavoproteins and cofactors that require regeneration, unlike the closely-related P450 monooxygenases.[11,12] *In vivo*, CPO utilizes H_2O_2 to perform oxidative halogenation reactions *via* hypohalous acid formation. *In vitro*, CPO exhibits a broad spectrum of synthetically valuable oxygen-transfer activity, including allylic, propargylic, and benzyl hydroxylation, asymmetric olefin epoxidation, and sulfoxidation with high regio- and *enantio*-selectivity.[13–21] As such, biocatalytic CPO applications in pharmaceutical synthesis, pollution remediation, and analytical diagnosis have been explored.[22–24] In the context of this study, CPO offers exceptional regioselectivity for the oxidation of indole derivatives to the corresponding 2-oxindole.[25–27]

However, the synthetic potential of CPO has been limited by its susceptibility to oxidative inactivation in the presence of H_2O_2, even at modest concentrations (half-life of approximately 1 hour in 30 μM H_2O_2 in the absence of organic substrates).[28] Conventionally, this challenge has been circumvented *via* the continuous addition of pre-formed commercial H_2O_2 to the reaction media.[28–30] Sheldon and coworkers demonstrated this strategy can offer exceptional peroxy-enzymatic performance, with 860 000 TTNs offered for CPO indole oxidation.[28] Despite offering improved enzymatic stability, this approach precludes CPO-based chemical transformations from operating at scale, owing to the rapid dilution of valuable product streams and concurrent production of excessive quantities of contaminated aqueous waste.[28,31] There are additional concerns regarding the energy inefficiency and cost associated with the manufacture, storage, and transport of commercial H_2O_2 *via* the Anthraquinone Oxidation Process.[32] As such, *in situ* H_2O_2 generation has the potential to offer a practical, atom-efficient, and environmentally benign solution to achieve the continuous low-concentration supply of oxidant required to maintain peroxy-enzymatic activity.[33]

Numerous *in situ* approaches to H_2O_2 supply for peroxy-enzymes have been developed, including photocatalytic, electrochemical, and multi-enzymatic cascades. Co-enzymatic approaches represent a well-established approach, with H_2O_2 generation *via* glucose oxidase (GOx), formate oxidase (FOx), and choline oxidase (ChOx) previously reported.[24,34,35] Despite offering high H_2O_2 production rates under enzymatically compatible reaction conditions, co-enzymatic strategies offer poor atom efficiency and undesirable by-product formation associated with the stoichiometric consumption of sacrificial co-reagents. The application of FOx minimises these drawbacks, however continual monitoring of the reaction media pH is required *via* acid titration, which could limit the process at scale. Photocatalytic H_2O_2 generation suffers from similar drawbacks, which rely on stoichiometric quantities of redox cofactors.[31,36] Exposure of the aqueous reaction media to UV radiation also results in the formation of reactive oxygen species (*e.g.* $^{\bullet}O_2^{-}$ and $^{\bullet}OH$), which are reported to contribute towards enzyme deactivation.[31] Holtmann *et al.* reported a highly efficient electrochemical H_2O_2 generation approach which employed a gas-diffusion electrode for O_2 reduction, offering 1 150 000 TTN for CPO 2-chloro-5,5-dimethyl-1,3-cyclohexanedione chlorination.[37] This clearly demonstrates the potential to achieve exceptional peroxy-enzymatic performance *via* the rapid generation and utilization of H_2O_2 *in situ*, however, such electrochemical approaches offer limited compatibility with current industrial reactor designs.

We have previously demonstrated the feasibility of a chemo-enzymatic approach, with supported AuPd nanoparticles employed to directly synthesise H_2O_2 *in situ* from molecular H_2 and O_2, coupled with an unspecific peroxygenase enzyme (UPO) from *Agrocybe aegerita* (PaDa-I variant), for selective C–H bond activation.[38–40] This approach offers highly atom efficient *in situ* H_2O_2 synthesis for biocatalytic utilization, while avoiding the use of sacrificial co-reagents and resulting side-product formation. However, high H_2O_2 direct synthesis reaction rates typically require sub-ambient temperatures, high pressure of gaseous reagents (>10 bar), and highly acidic reaction media (typically pH 4 or lower), which contrasts the near ambient conditions typically required to maintain enzyme activity.[41,42] Despite this, supported AuPd nanoparticles bridge this broad conditions gap, offering a continuous supply of H_2O_2 while maintaining peroxy-enzymatic activity, with both pressurized (2 bar) and atmospheric pressure reactor systems developed.[38–40]

Herein, we demonstrate the applicability of the chemo-enzymatic approach for the selective oxidation of indole *via* the coupling of supported AuPd nanoparticles and CPO from *Caldariomyces fumago* (Fig. 1). Highly efficient cascade efficiency was achieved by tuning the rate of chemo-catalytic H_2O_2 production with respect to peroxy-enzymatic utilization. Detailed investigation into dynamic nature of the chemo-catalytic component and the parameters driving enzymatic deactivation under cascade reaction conditions have facilitated the design of a highly compatible tandem system. Indeed, we elucidate the highly intertwined nature of chemo- and bio-catalysts under one-pot reaction conditions, wherein optimisation of the tandem system requires detailed understanding of the complex interplay of the cooperating components.

Experimental

Catalyst preparation

A series of 1 wt% Au_xPd_y/TiO_2 (where $Au:Pd = x:y$ by wt.), catalysts have been prepared *via* a sol-immobilization procedure, based on methodology reported previously in the literature, which has been shown to result in highly dispersed metal species by limiting particle growth and agglomeration.[43] The experimental procedure to produce the 1% Au_1Pd_1/TiO_2 (1 g) catalysts is outlined below (where the $Au:Pd$ wt. ratio is fixed at 1:1), with an analogous methodology employed to prepare the mono- and bi-metallic catalysts investigated in this study.
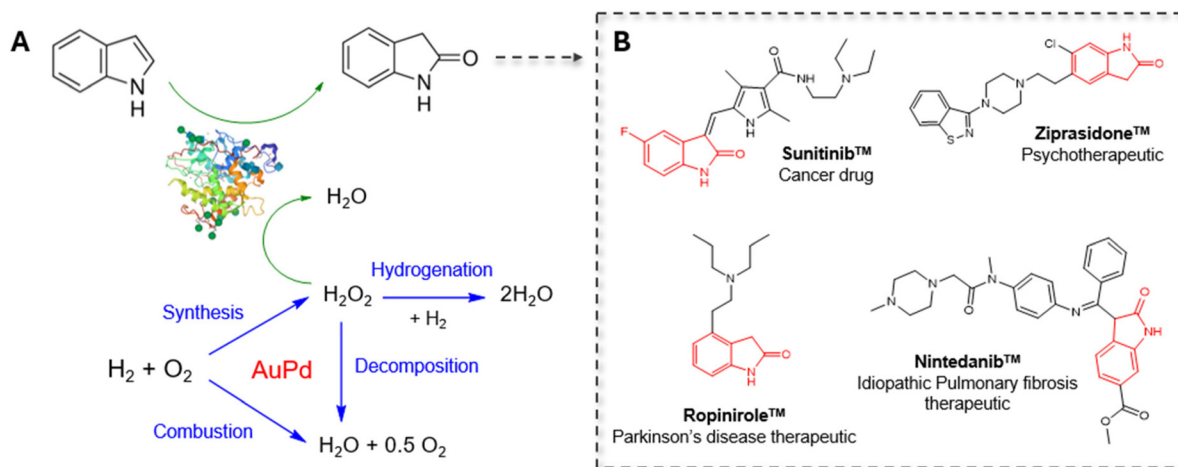
Fig. 1 (A) Proposed reaction scheme for the chemo-enzymatic oxidation of indole oxidation with chloroperoxidase and supported AuPd nanoparticles. (B) Active pharmaceutical ingredients containing the 2-oxindole scaffold. *Key*: (A) chemo-catalytic pathways (blue), enzymatic pathways (green).

Aqueous metal salt precursor solutions of $HAuCl_4$ (0.454 mL, [Au] = 11 mg mL^{-1}, Strem Chemicals) and $PdCl_2$ (0.714 mL, [Pd] = 7 mg mL^{-1}, Merck) were added to 400 mL deionised water and stirred at 1000 rpm. The requisite amount of PVA solution (1.3 mL, 1 wt% aqueous solution, MW = 10 000, 80% hydrolysed, Merck), was added to achieve a weight ratio of PVA : [Au + Pd] = 1.3. A freshly prepared solution of $NaBH_4$ (3.618 mL, 0.1 M, >98%, Merck), was added to the solution such that the molar ratio of $NaBH_4$: [Au + Pd] = 5. The solution was stirred for 30 min to allow for colloidal formation, before steady addition of TiO_2 (P25, 0.99 g, Degussa), followed by acidification to pH 1 using H_2SO_4 (95%, Fisher Scientific). After a further 1 hour of stirring, the slurry was filtered under vacuum and the resulting catalyst was washed with 2 L of deionised water, ensuring washings of neutal pH, and then dried (110 °C, 16 h). The dried catalyst was then collected and ground before calcining in static air (400° C, 3 h, ramp rate = 10 °C min^{-1}).

Catalyst testing

Note 1: in all cases, reactions were run multiple times, over multiple batches of catalyst, with the data being presented as an average of these experiments. Catalytic activity was found to be consistent to within ±5% on the basis of multiple reactions.

Note 2: reaction conditions used within this study operate outside the flammability limits of gaseous mixtures of H_2 and O_2.[44]

Chemo-catalytic H_2O_2 synthesis from H_2 and O_2

Reactions were conducted in 50 mL gas-tight round-bottom flasks rated to 4.1 bar and stirred using a Radleys 6 Plus Carousel equipped with a gas distribution system. The catalyst (0.001 g) was weighed directly into the round bottom flask before charging with reaction solution (10 mL). The reaction solvent was prepared by combining potassium phosphate buffer (KH_2PO_4/K_2HPO_4, Merck) with t-BuOH (>99%, Merck) in

a 1 : 1 ratio by volume (10 mM, pH 5.0 K_2HPO_4/KH_2PO_4 buffer with 50 vol% t-BuOH). Subsequently, the flasks were sealed, purged, and pressurized to 2 bar with H_2 (1.6 bar) and air (0.4 bar) to give a reaction environment containing 80% H_2 in air. The reactions were stirred at 250 rpm at ambient temperature (20 °C) for a given reaction time (5–180 min). Upon completion of a reaction, the glassware was depressurized and the spent catalyst was removed by filtration, before H_2O_2 concentrations were determined *via* UV/vis spectroscopy. To determine H_2O_2 concentration, an aliquot (1.5 mL) of post-reaction was combined with potassium titanium oxalate dihydrate solution acidified with 30% H_2SO_4 (0.02 M, 1.5 mL), resulting in the formation of an orange pertitanic acid complex. The resulting solution was analysed using a Shimadzu UV/vis 1900i spectrophotometer at 400 nm, with H_2O_2 concentrations determined by comparison to a calibration curve.

Chemo-catalytic degradation of H_2O_2

Catalytic activity toward H_2O_2 degradation (*via* hydrogenation and decomposition pathways), was determined in a similar manner to the above outlined H_2O_2 synthesis testing protocol, based on a previously established procedure.[39] The 50 mL gas-tight round bottom flasks were charged with the reaction solvent (10 mL, 10 mM, pH 5.0 K_2HPO_4/KH_2PO_4 buffer with 50 vol% t-BuOH) and H_2O_2 (2000 ppm, Merck). From the solution, prior to the addition of the catalyst, two 0.05 g aliquots were removed to allow for the quantification of the initial H_2O_2 concentration *via* UV–vis spectroscopy. Subsequently, the catalyst (0.001 g) was added to the flask, which was then sealed, purged, and pressurized to 2 bar with H_2 (1.6 bar) and N_2 (0.4 bar) to give a reaction atmosphere containing 80% H_2 and 20% N_2. The reaction mixtures were stirred (250 rpm) at ambient temperature (20 °C) for 2 h. After the desired reaction time, the vessel was depressurized, the catalyst was removed *via* filtration, and the remaining H_2O_2 was quantified by UV–vis spectroscopy.

Chemo-enzymatic indole oxidation

Reactions were conducted in 50 mL gas-tight round-bottom flasks rated to 4.1 bar and stirred using a Radleys 6 Plus Carousel equipped with a gas distribution system. Indole ($\geq$99%, Merck) was dissolved the reaction solvent (10 mL, 10 mM, pH 5.0 potassium phosphate buffer with 50 vol% t-BuOH) to give the desired substrate concentration (10 mM). The catalyst (0.001–0.004 g) was weighed directly into the 50 mL gas-tight round bottomed flasks, before charging with the prepared reaction mixture and CPO enzyme (15 U mL^{-1}, 600 nM, Merck). The flasks were immediately sealed and pressurized to 2 bar (80% H_2 in air), as described above. The reaction mixtures were stirred (250 rpm) at ambient temperature (20 °C) for the desired reaction time (15–180 minutes) before post-reaction analysis was conducted.

Filtered post-reaction aliquots were subjected to High-performance Liquid Chromatography (HPLC) analysis to monitor substrate conversion and product formation using an Agilent 1200 series equipped with an Agilent Poroshell 120 EC-C18 (2.7 µm 4.6 × 150 mm) column and Agilent 1260 series DAD detector at 278 nm. A water/acetonitrile mobile phase was employed with a gradient elution (0.75 mL min^{-1}, mobile phase ramped from 70 : 30 v/v to 50 : 50 v/v at 4–14 min). To quantify post-reaction concentrations of indole and 2-oxindole, calibrations were conducted with indole ($\geq$99%, Merck) and 2-oxindole (97%, Merck) commercial standards, allowing concentration determination of indole and 2-oxindole by comparison to a known response factor. Residual H_2O_2 concentration was determined following extraction of organic components with ethyl acetate (2 × 10 mL), before subjecting aliquots of the aqueous later to UV/vis spectroscopy. Unfiltered post-reaction aliquots were subjected to monochlorodimedone (MCD) assays to determine post-reaction enzyme activity, followed by appropriate application of an assay inhibition model (see experimental methods).

CPO activity measurements – monochlorodimedone (MCD) assay

CPO activity was determined via the MCD (2-chloro-5,5-dimethyl-1,3-cyclohexanedione, Fisher Scientific, 98%) assay, based on a previously established procedure reported in the literature, using the Shimadzu UV/vis 1900i spectrophotometer.[45] CPO solution (100 µL) was added to the MCD assay reaction mixture (900 µL, 100 mM potassium phosphate buffer, pH 2.75, 0.1 mM MCD, 20 mM KCl, 2 mM H_2O_2) and substrate conversion was followed by measuring the absorbance of MCD at 278 nm ($\varepsilon_{278} = 12\,200$ M^{-1} cm^{-1}) at 25 °C. The CPO solution was appropriately diluted to give linear enzyme kinetics. One activity unit (1 U) is defined as 1 µmol MCD converted in 1 min.

For more information regarding experimental details, including catalyst testing, analytical methods, and catalyst characterization, please see SI.

Results and discussion

Chemo-catalyst design for peroxy-enzymatic utilization

Our initial investigations aimed to establish chemo-enzymatic indole oxidation reaction conditions which optimized H_2O_2 synthesis rates, metal stability, and indole solubility (Fig. S1–10 and Tables S1, 2). Following this, we evaluated the efficacy of a 1% Au$_x$Pd$_y$/TiO$_2$ (where Au : Pd = $x : y$ by wt.) catalyst series, prepared by a previously established sol-immobilization method,[43] towards the direct synthesis and subsequent degradation of H_2O_2 under the optimized reaction conditions (Fig. 2A and B).[41] Chemo-catalytic H_2O_2 production was assessed over extended reaction times (up to 3 h), with the initial rate of H_2O_2 synthesis determined following 5 minutes reactions, where it is possible to exclude contributions from
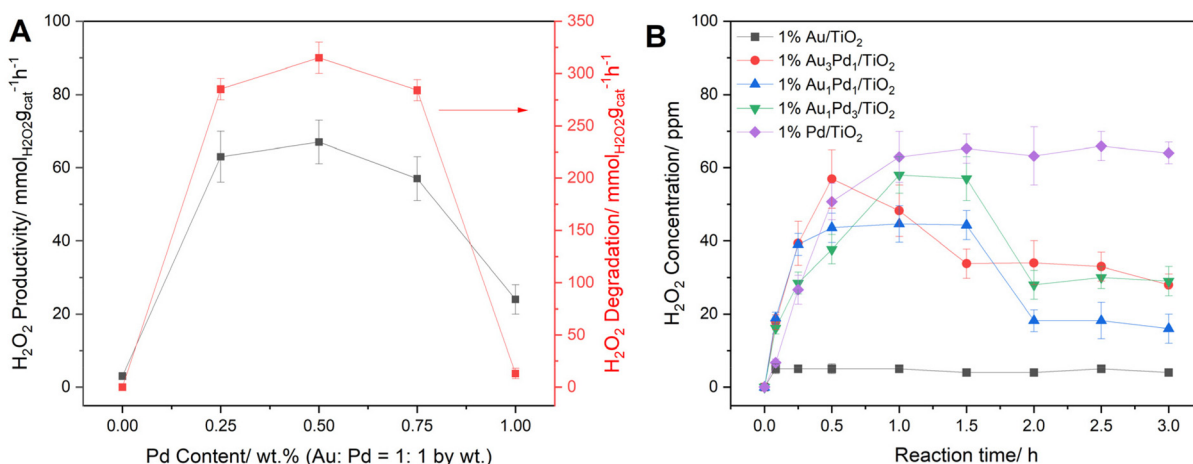

Fig. 2 Catalytic activity of the 1% Au$_x$Pd$_y$/TiO$_2$ series towards H_2O_2 synthesis and degradation. (A) H_2O_2 productivity and degradation determined over 5 minutes and 2 h reactions, respectively. (B) H_2O_2 production determined as a function of reaction time. *H_2O_2 synthesis reaction conditions*: catalyst (0.001 g), 2 bar (80% H_2 in air), potassium phosphate buffer (10 mM, 10 mL, pH 5.0) with 50 vol% t-BuOH, 250 rpm, 20 °C, 0–3 h. *H_2O_2 degradation reaction conditions*: catalyst (0.001 g), H_2O_2 (2000 ppm), 2 bar (80% H_2 in N_2), potassium phosphate buffer (10 mM, 10 mL, pH 5.0) with 50 vol% t-BuOH, 250 rpm, 20 °C, 2 h. *Note*: error bars within the boundary a given data point are not observable.

competitive degradation pathways or reagent limitation concerns (Fig. 2A). We have previously identified the initial rate of H_2O_2 synthesis as a key performance metric to understand chemo-catalyst efficacy when utilized in peroxy-enzymatic tandem systems.[39,40] However, it is clear that one must consider the limitations of such an approach, given the potential for dynamic chemo-catalyst performance over extended reaction times.

In keeping with previous reports, the incorporation of Au into Pd domains offered enhanced H_2O_2 synthesis rates (57–67 $mmol_{H_2O_2}$ g_{cat}^{-1} h^{-1} for bimetallic formulations), relative to the monometallic counterparts (3 and 24 $mmol_{H_2O_2}$ g_{cat}^{-1} h^{-1} for the Au and Pd monometallic analogues, respectively).[46–48] Such improvements have previously been attributed to the ability of Au to electronically modify Pd species and disrupt contiguous Pd ensembles.[49,50] Indeed, the performance of immobilized Pd-based catalysts towards H_2O_2 direct synthesis is known to be highly dependent on Pd speciation, with Pd^{2+} species typically reported to offer high selectivity while Pd^0 offer higher activity.[51–53] XPS analysis of the as-prepared 1% Au_xPd_y/TiO_2 catalyst series (Fig. S11 and Table S3), revealed that the 1% Pd/TiO_2 formulation consisted of predominately Pd^{2+} surfaces, which can be attributed to the employed oxidative heat treatment (static air, 400 °C, 3 h, 10 °C min^{-1}).[54] Upon incorporation of Au a shift towards Pd^0 was observed, indicating electronic modification of Pd species upon alloy formation, which correlates with the observed enhanced catalytic performance of the AuPd formulations. However, it is important to note that XPS analysis of the as-prepared formulations is not representative of the metal species *in situ*, particularly given the highly reducing nature of the reaction environment (80% H_2 in air).

Interestingly, evaluating H_2O_2 production over extended reaction times (3 h) revealed that the 1% Pd/TiO_2 formulation offered enhanced steady state activity towards H_2O_2 direct synthesis (6.3 $mmol_{H_2O_2}$ g_{cat}^{-1} h^{-1}), relative to the bimetallic AuPd analogues (1.6–2.8 $mmol_{H_2O_2}$ g_{cat}^{-1} h^{-1}) (Fig. 2B and Table S4). While this was not expected based on our initial rate measurements (Fig. 2A), this does align with the higher H_2O_2 degradation rates observed for the bi-metallic formulations, relative to the mono-metallic counterparts (0–13 and 284–315 $mmol_{H_2O_2}$ g_{cat}^{-1} h^{-1} for the mono- and bi-metallic catalysts, respectively) (Fig. 2A). However, given the rapid peroxy-enzymatic utilization, relative to H_2O_2 generation, chemo-catalytic H_2O_2 selectivity may be considered to be of limited concern in the tandem system. Indeed, we have previously demonstrated that under conditions where chemo-catalytic activity is rate-limiting, that is the rate of *in situ* H_2O_2 generation will govern the overall process efficiency of the tandem system.[39,40]

We subsequently evaluated the catalytic performance of the 1% Au_xPd_y/TiO_2 series when used in conjunction with CPO (600 nM, 15 U mL^{-1}) for the selective oxidation of indole to 2-oxindole *via in situ* H_2O_2 synthesis (Fig. 3). The highest chemo-enzymatic cascade efficacy was offered by the 1% Au_1Pd_1/TiO_2 catalyst, reflecting the enhanced initial rate of

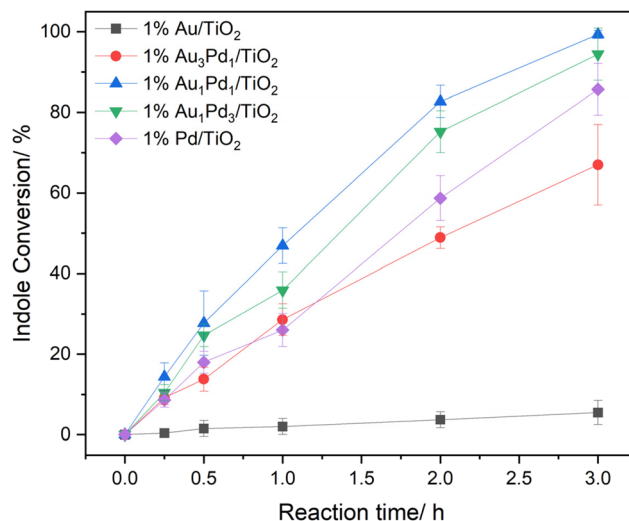**Fig. 3** Catalytic activity of the 1% Au_xPd_y/TiO_2 series towards indole oxidation in conjunction with CPO, as a function of catalyst formulation. *Indole oxidation reaction conditions*: catalyst (0.001 g), CPO (600 nM, 15 U mL^{-1}), indole (10 mM), potassium phosphate buffer (10 mM, 10 mL, pH 5.0) with 50 vol% *t*-BuOH, 2 bar (80% H_2 in air), 250 rpm, 20 °C, 0–3 h.

H_2O_2 synthesis offered by this formulation (Fig. 2A and Table S1). Notably, complete substrate conversion (>99% at 3 h) and exceptional selectivity towards 2-oxindole (93%) was achieved upon employing the 1% Au_1Pd_1/TiO_2 catalyst (Fig. S12). Importantly, each chemo-catalyst formulation offered 2-oxindole selectivity comparable to reported values for CPO with pre-formed H_2O_2, indicating the presence of the metal catalyst does not influence enzymatic selectivity under one-pot reaction conditions (Fig. S12).[26]

To investigate the selectivity of the tandem system further, we deconvoluted chemo-catalytic and enzymatic contributions towards unselective reaction pathways (Fig. S13, 14 and Table S5). Chemo-catalytic experiments (in the absence of CPO) revealed the 1% Au_xPd_y/TiO_2 catalyst series offered negligible activity towards indole oxidation and hydrogenation pathways, as well as 2-oxindole over-oxidation. While chemo-enzymatic experiments conducted with 2-oxindole revealed CPO contributions towards over-oxidation pathways (5% 2-oxindole conversion), indicating that the selectivity of the tandem system was enzymatically controlled (Fig. S14). Further control experiments established the significant improvement in indole oxidation activity achieved in the presence of H_2 and O_2, in comparison to that when either gaseous reagent (H_2 and O_2) was used separately (Table S6).

Notably, significantly higher indole oxidation rates were also observed *via* the chemo-enzymatic approach than could be achieved when utilizing pre-formed H_2O_2 at concentrations comparable to that offered by the chemo-catalyst (Table S7), where H_2O_2 was charged in a single injection to initiate the reaction. Further experiments were conducted *via* the continuous addition of *ex situ* H_2O_2 from an external reservoir (1.36 mM) using a perastaltic pump (50 mL h^{-1}), where

oxidant supply rates were aligned with chemo-catalytic H_2O_2 synthesis rates over the 1% Au_1Pd_1/TiO_2 (1.1 $\mu mol_{H_2O_2}$ min^{-1}) (Fig. S15A and B). The pump rate was selected in alignment with previous studies which utilize continuous oxidant addition, allowing appropriate benchmarking of chemo-enzymatic system.[28] Despite offering improved enzymatic performance and substrate turnover rates, relative to the single injection of H_2O_2, the rapid dilution of valuable reaction products and generation of excessive solvent waste is of significant concern when considering the green credentials and economic viability of this stategy (Fig. S15B). Additional experiments were conducted which employed GOx for *in situ* H_2O_2 generation (Fig. S15C), however enzymatic turnover rapidly reached extinction. Such deactivation can be associated with gluconic acid formation at 1 : 1 molar ratio with H_2O_2, resulting in a rapid acidification of the reaction media under the weakly buffered reaction conditions (pH 5.0, 10 mM potassium phosphate buffer). This further highlights the improved co-catalyst stability offered by the chemo-catalytic approach, hence facillitating a broader operating window for *in situ* H_2O_2 synthesis.

Evolving chemo- and bio-catalytic activity under reaction conditions

Upon closer inspection of the chemo-enzymatic indole oxidation rates offered by the 1% Au_xPd_y/TiO_2 catalysts (Fig. 3), the Pd-rich formulations were found to offer significantly higher cascade activity, relative to the Au-rich analogues, than could have been predicted based on measurements of initial H_2O_2 production rates (Fig. 2A and Table S1). Given the disparate reaction times at which H_2O_2 synthesis (5 minutes) and indole oxidation (3 h) experiments were conducted, we were motivated to investigate the potential evolution of chemo-catalytic activity under reaction conditions. We subsequently measured the initial rate of H_2O_2 synthesis of the 1% Au_xPd_y/TiO_2 catalyst series over multiple uses (Fig. S16), revealing increased activity of the Pd-rich formulations following exposure to reaction conditions, which correlates with the exceptional tandem performance offered by these catalysts. Interestingly, the 1% Au_3Pd_1/TiO_2 formulation exhibited a significant reduction towards H_2O_2 synthesis rates over multiple uses (57% activity reduction upon third use), which aligns with the comparatively poor chemo-enzymatic efficacy offered by this formulation. ICP-MS analysis of post-reaction solutions (Table S.2) demonstrated minimal leaching of metal species (≤0.1% Pd leaching for the 1% Au_xPd_y/TiO_2 series, Au leaching was not observed), suggesting chemo-catalytic deactivation cannot be attributed to loss of active metal species. Interestingly, XPS analysis of the 1% Au_xPd_y/TiO_2 catalysts revealed a complete shift towards Pd^0 species following model H_2O_2 synthesis reactions, which were conducted with ten times the typical catalyst mass (0.01 g), and in the absence of CPO and indole (Fig. S17). Such findings highlight the dependency of tandem performance on the dynamics of chemo-catalytic activity under reaction conditions.

To explore the temporal dependence of Pd speciation under reaction conditions, further model H_2O_2 synthesis experiments were conducted over a range of reaction times (5–60 minutes), with a particular focus on the 1% Au_1Pd_1/TiO_2 and 1% Pd/TiO_2 formulations (Fig. 4B and Fig. S18). Interestingly, a rapid shift towards Pd^0 was observed within 5 minutes of reaction for both catalysts, revealing that Pd^0 is the prevailing chemo-catalytically active species under cascade conditions. Such findings indicate the enhanced CPO turnover rates achieved in conjunction with the Pd-rich formulations (Fig. 3), relative to the Au-rich catalyst, correspond with an enhanced proportion of surface Pd^0 species and consequently promoted H_2O_2 direct synthesis activity. However, under circumstances where H_2O_2 productions rates are solely governed by surface Pd^0 species, one would predict the 1% Pd/TiO_2 formulation to offer the highest efficacy in the tandem system. Therefore, the role of AuPd species in maintaining high H_2O_2 synthesis rates is considered critical, as highlighted by the enhanced indole oxidation rates offered by the 1% Au_1Pd_1/TiO_2 formulation, relative to the 0.5% Pd/TiO_2 monometallic counterpart (83% and 33% indole conversion for 1% Au_1Pd_1/TiO_2 and 0.5% Pd/TiO_2 catalyst at 2 h, respectively) (Table S6). Such findings underpin the critical requirement to design chemo-catalysts which offer high H_2O_2 synthesis activity, rather than high H_2O_2 selectivity, under tandem conditions which impose chemo-catalytic activity as rate-limiting, relative to peroxy-enzymatic utilization.

Building further on these studies, and with a focus on the 1% Au_1Pd_1/TiO_2 formulation, we next investigated the influence of evolving chemo-catalytic activity towards tandem performance (Fig. S19). Such studies first exposed the chemo-catalyst to model H_2O_2 synthesis reaction conditions over a standard 2 h reaction, prior to subsequent use in the chemo-enzymatic cascade. Notably, these studies revealed the instability of the chemo-catalyst with a considerable loss in indole conversion, compared to that observed when utilising the as-prepared catalyst (4660 h^{-1} and 2860 h^{-1} for the fresh and used catalyst at 2 h, respectively). This contrasts our earlier studies, which established that chemo-catalytic activity towards H_2O_2 was maintained upon exposure to reaction conditions (Fig. S16). However, it is important to note H_2O_2 direct synthesis experiments conducted over extended reaction times also revealed a reduction towards H_2O_2 production upon chemo-catalyst reuse (Fig. S20). ICP-MS analysis of post-reaction solutions revealed the increased Pd leaching of the 1% Au_1Pd_1/TiO_2 catalyst upon second use (Table S8), relative to that observed upon initial exposure to the reaction conditions (0.1% and 0.7% Pd leaching upon first and second use for the catalyst at 2 h, respectively, Au leaching was not observed). While such findings clearly indicate increased mobility of the supported nanoparticles, such extensive chemo-catalytic deactivation cannot be entirely attributed to the observed Pd leaching.

To probe the surface morphology and structure of the 1% Au_1Pd_1/TiO_2 formulation, HAADF AC-STEM X-EDS analysis was conducted on the fresh and used catalyst, following a model H_2O_2 synthesis reaction over 2 h (Fig. 4A, with additional data reported in Fig. S21–28). X-EDS imaging revealed the presence
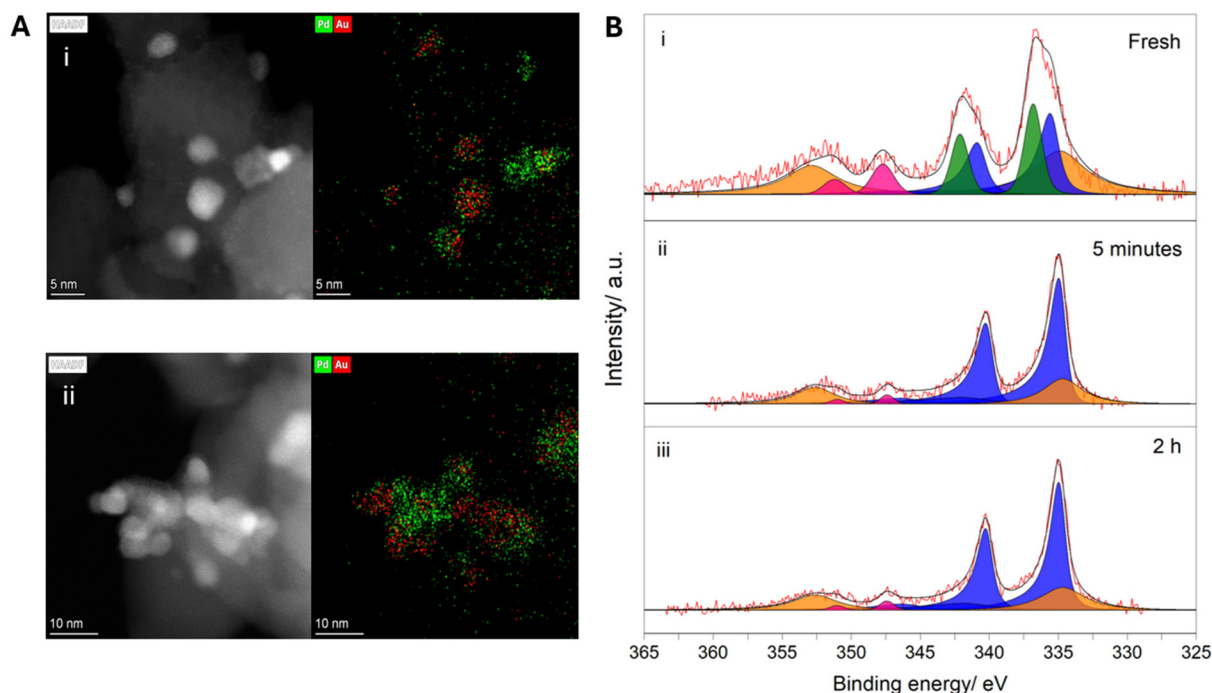
Fig. 4 Structure and morphology of the 1% Au_1Pd_1/TiO_2 catalyst. (A) HAADF AC-STEM X-EDS imaging of the as-prepared (i) and used (ii) catalyst, following a model H_2O_2 synthesis reaction over 2 h. (B) Surface atomic compositions in the Pd (3d) region of the as-prepared (i) and used catalyst (ii–iii), following a model H_2O_2 synthesis reaction over 5 minutes (ii) and 2 h (iii). *Key*: Au^0 (orange), Pd^0 (blue), Pd^{2+} (green), Ca^{2+} (pink). *Model H_2O_2 direct synthesis reaction conditions*: catalyst (0.01 g), 2 bar (80% H_2 in air), potassium phosphate buffer with 50 vol% *t*-BuOH (10 mM, pH 5.0, 10 mL), 250 rpm, 20 °C, 0.083–2 h.

of well-defined AuPd nanoalloy structures in the fresh catalyst, with particle sizes ranging from 2–10 nm, in addition to a population of Pd-rich nanoparticles ranging from 4–11 nm and highly dispersed sub-nano monometallic Pd species (Fig. S21–23). In contrast, the used 1% Au_1Pd_1/TiO_2 catalyst exhibited populations of large aggregates (≤50 nm), with the highly dispersed (<1 nm) monometallic Pd species absent, demonstrating significant nanoparticle agglomeration under reaction conditions (Fig. S24–28). Unsurprisingly, X-EDS imaging also revealed deposited K and P on the chemo-catalyst surface associated with surface adsorption from the potassium phosphate buffer (Fig. S27). As such, we attribute the observed loss of chemo-catalytic activity, and therefore chemo-enzymatic performance, to changes in nanoparticle structure and morphology under reaction conditions. These studies clearly highlight the need for improved approaches to chemo-catalyst design, with a particular focus on stability.

We subsequently investigated the evolution of enzymatic activity under reaction conditions, with monochlorodimedone (MCD) assays employed to determine CPO activity following chemo-enzymatic indole oxidation experiments with the 1% Au_xPd_y/TiO_2 catalyst series (Fig. S29). Given peroxidative inactivation proceeds concurrently with the conversion of substrate, CPO deactivation has been evaluated with respect to enzyme turnovers (Fig. 5A).[55,56] Interestingly, the extent of CPO deactivation was observed to be highly dependent on the chemo-catalyst formulation, with the Pd-containing and monometallic

Au catalysts resulting in disparate CPO deactivation profiles. Unsurprisingly, CPO deactivation proceeded steadily with substrate turnover when used in conjunction with Pd-containing formulations, associated with peroxy-enzymatic turnover. However, the extensive CPO deactivation observed upon utilizing the 1% Au/TiO_2 catalyst cannot be attributed to peroxidative inactivation, owing to the minimal H_2O_2 production rates and consequently poor cascade efficacy offered by this formulation. Such findings highlight the potential for CPO deactivation to proceed *via* non-peroxy-mediated pathways under chemo-enzymatic cascade reaction conditions. Importantly, contributions of the reaction substrates and products towards the measured CPO activity have been accounted for *via* an assay inhibition model (see experimental methods in the SI).

To begin deconvoluting contributions towards enzyme deactivation, CPO was exposed to the employed reaction parameters in a stepwise manner, in the absence of chemo-catalyst and indole substrate (Fig. 5B). While the key reaction parameters contributed minimal CPO deactivation when assessed individually (Fig. 5B, i–iii), the combination of the pressurized reaction environment (2 bar, 80% H_2 in air) and organic cosolvent (50 vol% *t*-BuOH) resulted in extensive CPO deactivation (77%, 3 h). Pressure-induced enzyme deactivation mechanisms have been reported to proceed *via* promoted exchange between protein bound water molecules and the bulk solvent environment.[57–59] We postulate such effects perpetuate CPO deactivation in this study, with enhanced *t*-BuOH penetration
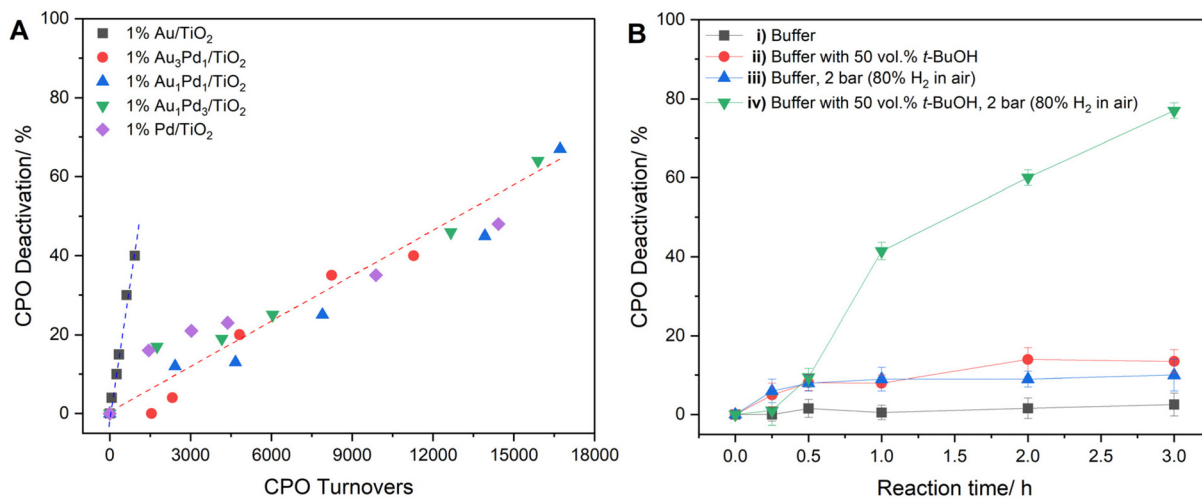
Fig. 5 Extent of CPO deactivation, as determined *via* the MCD assay. (A) Chemo-enzymatic indole oxidation reactions with 1% Au_xPd_y/TiO_2 catalysts. (B) CPO deactivation as a function of reaction conditions, as determined *via* the MCD assay, in the absence of the chemo-catalyst and indole. (A) *Indole oxidation reaction conditions*: catalyst (0.001 g), CPO (600 nM, 15 U mL^{-1}), indole (10 mM), potassium phosphate buffer (10 mM, 10 mL, pH 5.0) with 50 vol% *t*-BuOH, 2 bar (80% H_2 in air), 250 rpm, 20 °C, 0–3 h. (B) *Reaction conditions*: (i) CPO (600 nM, 15 U mL^{-1}), potassium phosphate buffer (10 mL, 10 mM, pH 5.0), ambient pressure, 20 °C, 250 rpm, 0–3 h. (ii) CPO (600 nM, 15 U mL^{-1}), potassium phosphate buffer (10 mL, 10 mM, pH 5.0) with 50 vol% *t*-BuOH, ambient pressure, 20 °C, 250 rpm, 0–3 h. (iii) CPO (600 nM, 15 U mL^{-1}), potassium phosphate buffer (10 mL, 10 mM, pH 5.0), 2 bar (80% H_2 in air), 20 °C, 250 rpm, 0–3 h. (iv) CPO (600 nM, 15 U mL^{-1}), potassium phosphate buffer (10 mL, 10 mM, pH 5.0) with 50 vol% *t*-BuOH, 2 bar (80% H_2 in air), 20 °C, 250 rpm, 0–3 h. *MCD assay reaction conditions*: post-reaction aliquot (100 μL), assay solution (900 μL, 0.1 mM MCD, 20 mM KCl in 100 mM, pH 2.75 potassium phosphate buffer), absorbance monitored at 278 nm (ε_{278} = 12 200 M^{-1} cm^{-1}), 25 °C.

into the protein bonding network at elevated pressure driving the observed hydrophobic/pressure co-action effect.

To investigate the potential for metal species to contribute towards enzyme deactivation, model studies were conducted to expose CPO to leached metal species from the 1% Au_1Pd_1/TiO_2 catalyst and metal chloride salts at various concentrations ($PdCl_2$, $HAuCl_4$) (Table S9). Such experiments were conducted in an aqueous buffer system (10 mL, 10 mM, pH 5.0 potassium phosphate buffer) at ambient pressure, thus removing pressure and organic solvent contributions towards CPO deactivation. We previously reported the capacity of homogenous metal species to deactivate a closely-related UPO enzyme,[40] however, CPO exhibited excellent stability in the presence of aqueous metal species.

Optimization of the tandem system and substrate scope

Following our initial studies, the 1% Au_1Pd_1/TiO_2 formulation emerged as the most promising chemo-catalyst candidate for application in the tandem system. To enable further improvements of the overall process efficiency, we optimised the kinetic balance between *in situ* H_2O_2 production rates and subsequent peroxy-enzymatic utilization. With a particular focus on the 1% Au_1Pd_1/TiO_2 formulation, the chemo-catalyst: enzyme ratio was modified by increasing the mass of chemo-catalyst employed, facilitating a simple approach to promote *in situ* H_2O_2 synthesis rates (Fig. 6A and Fig. S30). Interestingly, enzymatic TOF scaled linearly with increased chemo-catalyst mass from 1 to 3 mg (Fig. S31), reaching a maxima of 18 600^{-1} when utilising the highest catalyst mass, with near full indole conversion achieved (98% conversion,

92% selectivity to 2-oxindole) after 1 h of reaction. These observations further highlight the high oxidant utilization efficiency of the enzyme, as well as the limited contribution of unselective H_2O_2 consumption *via* chemo-catalytic degradation pathways.

Further increasing chemo-catalyst mass to 4 mg offered the highest initial enzymatic TOF (23 300 h^{-1} at 0.5 h), however substrate turnover could not be maintained and rapidly reached extinction (76% conversion, 0.75 h). Evaluation of post-reaction enzyme activity (Fig. 6B) revealed this was accompanied with complete enzyme deactivation (100% deactivation, 0.75 h), indicating *in situ* H_2O_2 production rates exceeded that of peroxy-enzymatic utilization, resulting in rapid oxidative inactivation. This aligns with findings from chemo-enzymatic experiments conducted in the absence of indole, which revealed significantly increased CPO deactivation rates upon switching-off enzymatic oxygen transfer pathways (Fig. S32). Such effects are associated with the characteristic catalase (H_2O_2 degradation) activity of CPO, which is prone to malfunction in the presence of excess oxidant, resulting in enzyme active site denaturing *via* 'heme-bleaching'.[55,60,61] As such, this work demonstrates that the promotion of cascade efficacy *via* enhanced H_2O_2 synthesis rates must operate under chemo-catalytic rate limitations to maintain enzymatic activity.

To probe the potential for *in situ* enzyme physisorption onto the chemo-catalyst surface, post-reaction CPO activity was assessed in filtered and unfiltered post-reaction aliquots, allowing free and immobilized enzyme contributions to be deconvoluted (Fig. S33). With a particular focus on the 1%
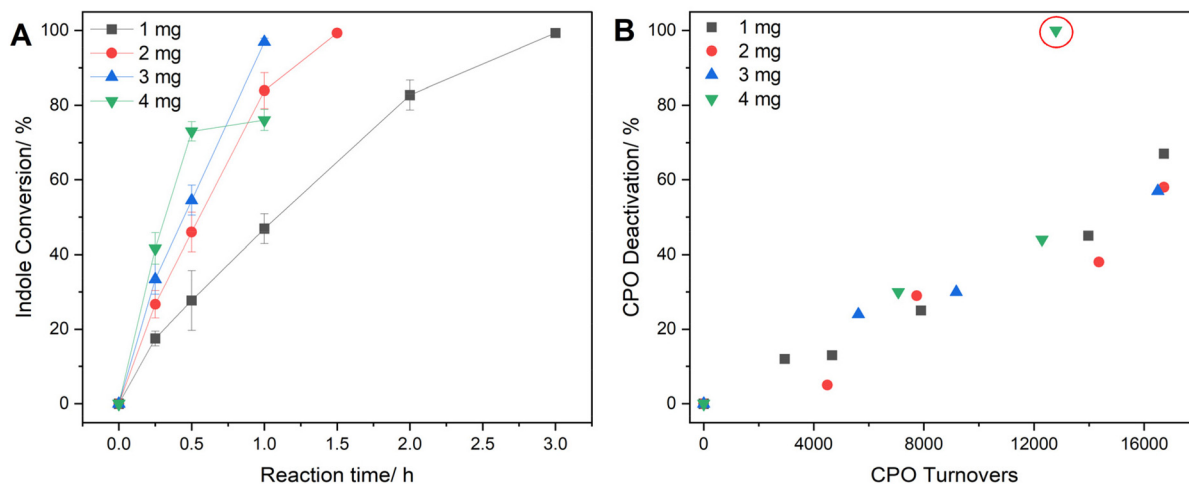
Fig. 6 (A) Catalytic activity of 1% Au_1Pd_1/TiO_2 towards indole oxidation, when used in conjunction with CPO, as function of chemo-catalyst mass. (B) Extent of CPO deactivation, as a function of CPO turnovers, following indole oxidation reactions with varying chemo-catalyst mass. *Indole oxidation reaction conditions*: catalyst (0.001–0.004 g), CPO (600 nM, 15 U mL^{-1}), indole (10 mM), 2 bar (80% H_2 in air), potassium phosphate buffer (10 mM, 10 mL, pH 5.0) with 50 vol% *t*-BuOH, 250 rpm, 20 °C, 0–3 h. *MCD assay reaction conditions*: post-reaction aliquot (100 μL), assay solution (900 μL, 0.1 mM MCD, 20 mM KCl in 100 mM, pH 2.75 potassium phosphate buffer), absorbance monitored at 278 nm (ε_{278} = 12 200 M^{-1} cm^{-1}), 25 °C. Note: Red circle indicates complete enzyme deactivation upon utilizing 4 mg chemo-catalyst.

Au_1Pd_1/TiO_2 catalyst at loadings of 1 mg and 3 mg, CPO was exposed to key reaction parameters (2 bar N_2, 10 mL, 10 mM, pH 5.0 potassium phosphate buffer with 50 vol% *t*-BuOH), in the absence of indole and H_2O_2 synthesis reagent gases, which switched-off peroxy-enzymatic turnover. Interestingly, immobilized enzyme accounted for 23% of post-reaction CPO activity when utilizing 1 mg chemo-catalyst, which raised to 58% at 3 mg. Notably, increased enzyme immobilization was accompanied with suppressed CPO deactivation, suggesting *in situ* physisorption effects mediate enzyme stabilization under the employed reaction conditions. Muñoz-Guerrero *et al.* reported similar findings, demonstrating enhanced operational stability of CPO following physical immobilization on TiO_2 nanotubes, with the immobilized enzyme offering a 69% improvement in TTN, relative to the free enzyme.[62] Such findings highlight the complex interplay between peroxidative inactivation and physical stabilization upon varying chemo-catalyst mass, wherein an optimized tandem system carefully balances such effects.

Hitherto, enzymatic turnovers have been limited to 16 670 under chemo-enzymatic cascade conditions, owing to the selected substrate concentration (indole, 10 mM). To demonstrate the capacity of the tandem system to achieve higher TTN, a series of substrate recharging experiments were performed, with a continued focus on the 1% Au_1Pd_1/TiO_2 formulation (Fig. 7 and Fig. S34). Such experiments were carried out with 1, 2, and 3 mg chemo-catalyst, allowing the TTN to be probed as a function of *in situ* H_2O_2 production rate. For each of the systems investigated, substrate recharging (2 bar, 80% H_2 in air, 10 mM indole) was conducted at intervals equal to the reaction time required to reach near total conversion of indole (as reported in Fig. 6A, *e.g.* the 1 mg chemo-catalyst experiment was re-charged at 3 h intervals). Interestingly, the
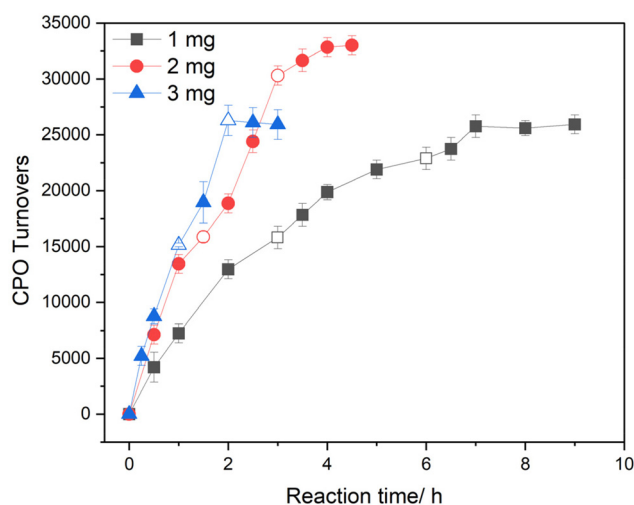

Fig. 7 Catalytic activity of 1% Au_1Pd_1/TiO_2 towards indole oxidation, when used in conjunction with CPO, as a function of chemo-catalyst mass, probed *via* substrate recharging experiments. *Indole oxidation reaction conditions*: 1% Au_1Pd_1/TiO_2 (0.001–0.003 g), CPO (600 nM, 15 U mL^{-1}), indole (10 mM), potassium phosphate buffer (10 mL, 10 mM, pH 5.0) with 50 vol% *t*-BuOH, 2 bar (80% H_2 in air), 20 °C, 250 rpm, 0–3 h. *Note*: Reaction time at which substrate recharging (indole and reagent gases) was conducted indicated by hollow data points.

resulting enzymatic TTN was highly dependent on the rate of *in situ* H_2O_2 production, with 2 mg of chemo-catalyst offering the highest enzymatic efficacy (25 000, 33 000, and 25 900 TTN for 1, 2, and 3 mg chemo-catalyst, respectively), corresponding to 19.6 mM of 2-oxindole formation in 3 h. As such, the reported chemo-enzymatic cascade offers highly competitive CPO TTN for indole oxidation, particularly when compared to

previously reported systems which exploit *in situ* generated H_2O_2 *via* co-enzymatic and electrochemical approaches (Table S10).[63,64] The relative performance of the chemo-catalyst masses investigated is rationalized by considering the trade-off between enzyme TOF and peroxidative inactivation, as a function of H_2O_2 production rate, while the extent of physical stabilization at varying chemo-catalyst masses should also be considered. Indeed, this study further highlights the enhanced enzymatic performance that can be offered *via* the chemo-enzymatic approach, owing to the highly tuneable nature of *in situ* H_2O_2 production rates.
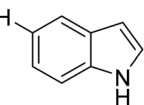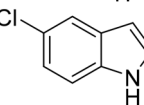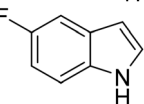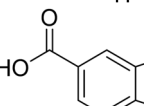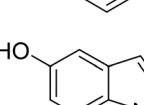
The developed chemo-enzymatic system was subsequently utilized for the selective oxidation of a range of substituted indoles, chosen for their unique electronic and structural characteristics, allowing the specificity of the tandem system to be assessed. Such experiments were conducted with the 1% Au_1Pd_1/TiO_2 (1 mg) formulation over a standard 2 h reaction (Table 1 and Table S11). Interestingly, CPO offered reduced oxidation activity towards substituted substrates. Van Deurzen *et al.* reported analogous findings upon utilizing pre-formed H_2O_2 for CPO-mediated synthesis of substituted oxindoles.[26] Indeed, the presence of substituent at the indole C-3–7 positions has been reported to sterically hinder access to the heme active site *via* the narrow hydrophobic channel, relative to non-substituted indole. It is also important to consider the electronic effects of substituents on the resonance stabilized

radical cation indole intermediate species in the oxidative mechanism.[25] In keeping with our findings thus far, both the chemo-catalytic activity towards the indole-derivatives was not observed and the supply of *ex situ* H_2O_2 offered significantly lower enzymatic efficacy than *in situ* generated oxidant (Table S11). Such findings highlight that the versatile nature of CPO-based biocatalysis is maintained when coupled with supported AuPd catalysts under one-pot reaction conditions. However, the reduced chemo-enzymatic efficacy upon utilizing substituted indole is considered critical when designing synthetic routes towards target substrates.

Techno-economic analysis

We subsequently conducted a detailed techno-economic analysis of the materials employed for the chemo-enzymatic, co-enzymatic (GOx), and continuous H_2O_2 addition strategies (Fig. 8, additional data reported in Tables S12–15). Importantly, material cost has been determined for the key components in the generation of 1 ton of 2-oxindole, with the cost associated with post-reaction purification and solvent processing not accounted for in this analysis. Interestingly, the chemo-catalytic approach offered significantly improved economic potential, relative to the co-enzymatic and continuous addition approaches. Unsurprisingly, the co-enzymatic approach suffers from the combined high cost and poor stabi-

Table 1 Substrate scope of the chemo-enzymatic cascade for the synthesis of substituted 2-oxindoles

Substrate	Substrate conversion/%	2-Oxindole derivative selectivity/%	TON
H (indole)	83	95	13 970
Cl (5-chloroindole)	55	98	9 260
F (5-fluoroindole)	61	86	8 830
HOOC (indole-5-carboxylic acid)	24	99	4 040
HO (5-hydroxyindole)	32	83	4 470

Substituted Indole oxidation reaction conditions: 1% Au_1Pd_1/TiO_2 (0.001 g), CPO (600 nM, 15 U mL^{-1}), substrate (10 mM), potassium phosphate buffer (10 mM, 10 mL, pH 5.0) with 50 vol% *t*-BuOH, 2 bar (80% H_2 in air), 250 rpm, 20 °C, 2 h. Note: enzymatic performance reported as TON as experiments did not reach catalytic extinction.
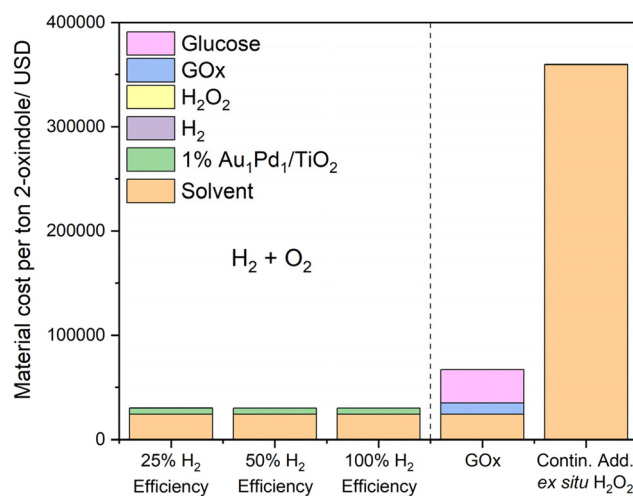

Fig. 8 *Continuous H_2O_2 addition reaction conditions*: H_2O_2 reservoir (1.36 mM), pump (50 mL h^{-1}), CPO (15 U mL^{-1}, 600 nM), indole (10 mM), potassium phosphate buffer (10 mL, 10 mM, pH 5.0) with 50 vol% *t*-BuOH, ambient pressure, 250 rpm, 20 °C, 0–3 h. *Co-enzymatic reaction conditions*: glucose oxidase (0.2 U mL^{-1}), glucose (100 mM), CPO (15 U mL^{-1}, 600 nM), indole (10 mM), potassium phosphate buffer (10 mL, 10 mM, pH 5.0) with 50 vol% *t*-BuOH, ambient pressure, 250 rpm, 20 °C, 0–3 h. *Chemo-enzymatic reaction conditions*: catalyst (0.001 g), CPO (15 U mL^{-1}, 600 nM), indole (10 mM), potassium phosphate buffer (10 mL, 10 mM, pH 5.0) with 50 vol% *t*-BuOH, 2 bar (80% H_2 in air), ambient pressure, 250 rpm, 20 °C, 0–3 h. *Note 1*: * indicates H_2 consumption has been calculated based on estimated H_2 utilization efficiencies with respect to 2-oxindole formation. *Note 2*: H_2O_2 (407 USD) and H_2 (30–120 USD) cost are not visually observable on the scale provided in the figure.
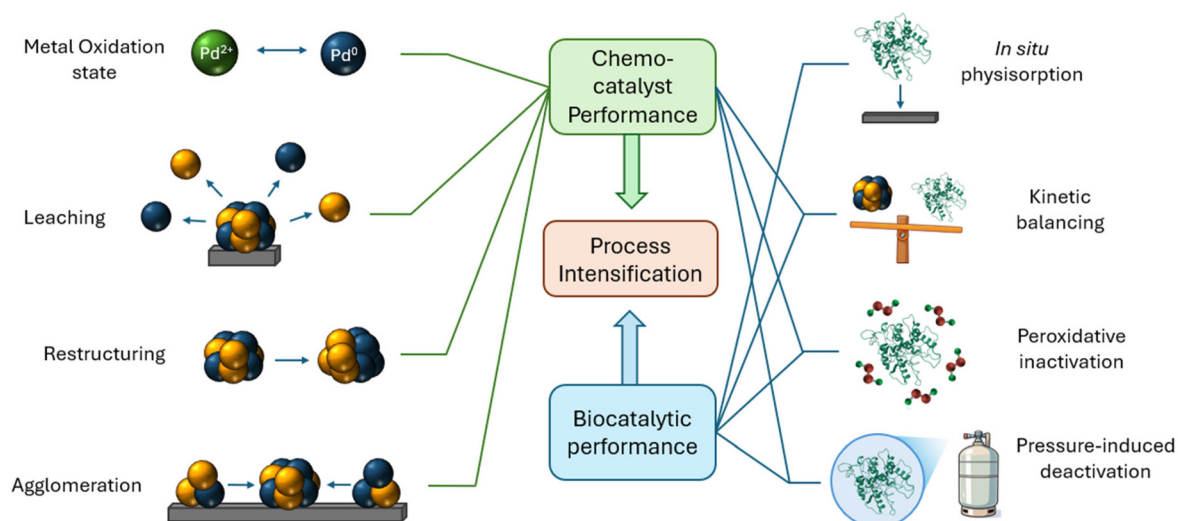
Green Chemistry

Paper

Fig. 9 Schematic representation of the critical parameters to optimise when combining chemo- and bio-catalysts for tandem system chemical transformations.

lity of GOx under reaction conditions, rendering this approach economically unviable. Commercial H_2O_2 offers lower cost than that of the chemo-catalyst and H_2 usage combined, however the requirement for excessive solvent to maintain dilute H_2O_2 streams hampers the economic potential of this approach. These drawbacks are further exacerbated by the high cost associated with downstream processing of contaminated solvent waste. Interestingly, this analysis aligns with the resulting *E*-factors (mass waste/mass product) for each of systems investigated (670, 11 470, and 3250 for the chemo-catalytic, continuous H_2O_2 addition, and co-enzymatic approaches, respectively) (Table S16), with further improvements obtained for the chemo-catalytic approach *via* substrate recharging experiments (*E*-factor = 340) (Fig. 7). In summary, the moderate cost of chemo-catalyst preparation is significantly offset by the comparatively low cost of H_2 and significantly reduced solvent usage, which exemplifies the exceptional green credentials and economic viability of this technology, relative to previously established H_2O_2 supply strategies for biocatalytic applications.

Conclusion

We have demonstrated the applicability of coupling chemo-catalytic generation of H_2O_2 and CPO to selectively oxidize indoles as an attractive route for the synthesis of pharmaceutically valuable products. The incorporation of Au into Pd nanoparticles offered significantly enhanced H_2O_2 synthesis rates, which facilitated kinetic optimization of *in situ* oxidant generation and peroxy-enzymatic utilization. Indeed, the 1% Au_1Pd_1/TiO_2 offered 33 000 TTN for selective indole oxidation to 2-oxindole, which is among the most efficacious CPO-based indole oxidation systems reported which utilize *in situ* generated H_2O_2.[63,64] Indeed, when compared to alternative *in situ* H_2O_2 production approaches for peroxy-enzymatic utilization,

the chemo-enzymatic approach has exceptional potential to be scaled for industrial applications, offering high atom efficiency, economic viability, and compatibility with current reactor technologies. Importantly, the characteristically exceptional regio- and chemo-selectivity of CPO was maintained under one-pot reaction conditions.

Despite offering highly efficient H_2O_2 generation and utilization, we have revealed the potential for chemo- and bio-catalytic deactivation under the tandem system reaction conditions. We have also demonstrated the dynamic nature of metal species, which is proposed to contribute towards the observed loss of chemo-catalytic activity over multiple uses. Therefore, for the chemo-enzymatic system to rival current industrial processes, further improvements in catalyst stability are required to maintain high chemo-catalytic activity over extended lifetimes.

We have also revealed the combination of a pressurized reaction environment and highly organic solvent environment results in extensive enzyme deactivation through an observed co-action effect. As such, efforts to improve the scalability and economic viability of the chemo-enzymatic cascade system should focus on enhancing enzyme stability under operating conditions. Numerous strategies to achieve such effects have been widely reported, with protein engineering, enzyme immobilization, and utilization of extremophilic enzymes representing viable approaches.[65–67] Indeed, this work has demonstrated improved enzyme stability following *in situ* physisorption at the chemo-catalyst surface, highlighting the potential for further enhancements *via* robust immobilization strategies, such as covalent anchoring. The development of a heterogeneous chemo-enzymatic tandem system would offer significant industrial and economic advantages, owing to improved ease of catalyst separation from post-reaction mixtures, as well as facilitating the design of continuous/semi-continuous reactor systems.[68,69]

In summary, through a holistic and detailed approach we have elucidated a complex array of critical chemo- and bio-catalytic parameters which must be considered to optimise chemo-enzymatic performance (as summarised in Fig. 9). As Gröger and coworkers describes, chemo-enzymatic catalysis imposes the selection of reaction conditions as crucial and evidently nontrivial, owing to the complexities associated with overcoming the conditions gap between chemo- and bio-catalytic components, which must be achieved to realise the vast synthetic potential of such tandem systems.[70] Indeed, this work highlights the dynamic nature of such catalytic phenomena under reaction conditions, with such understanding considered critical towards developing highly active, stable, and industrially feasible chemo-enzymatic tandem systems.

Author contributions

A. S. and J. P. conducted catalyst synthesis, testing, and corresponding data processing. A. S., R. J. L., D. J. M., T. E. D. conducted catalyst characterization and corresponding data processing. A. S., R. J. L., and G. J. H. contributed to the design of the study and interpretation. A. S. wrote the manuscript and SI, with all authors commenting on and amending both documents. All authors discussed and contributed to this work.

Conflicts of interest

The authors declare no conflict of interest.

Data availability

All data is available in the manuscript and the supplementary information (SI), which is available at DOI: https://doi.org/10.1039/d5gc05367f.

Acknowledgements

References

1 V. L. Goodman, E. P. Rock, R. Dagher, R. P. Ramchandani, S. Abraham, J. V. S. Gobburu, B. P. Booth, S. L. Verbois, D. E. Morse, C. Y. Liang, *et al.*, Approval summary: Sunitinib for the treatment of imatinib refractory or intoler-ant gastrointestinal stromal tumors and advanced renal cell carcinoma, *Clin. Cancer Res.*, 2007, **13**(5), 1367–1373.

2 M. Jörg, A. A. Kaczor, F. S. Mak, K. C. K. Lee, A. Poso, N. D. Miller, P. J. Scammells and B. Capuano, Investigation of novel ropinirole analogues: synthesis, pharmacological evaluation and computational analysis of dopamine D2 receptor functionalized congeners and homobivalent ligands, *MedChemComm*, 2014, **5**(7), 891–898.

3 F. J. Urban, R. Breitenbach and D. Gonyaw, A Novel Synthesis of the Antipsychotic Agent Ziprasidone, *Synth. Commun.*, 1996, **26**(8), 1629–1638.

4 R. Xu, M. Zhan, L. Peng, X. Pang, J. Yang, T. Zhang, H. Jiang, L. Zhao and Y. Chen, Design, synthesis and biological evaluation of deuterated nintedanib for improving pharmacokinetic properties, *J. Labelled Compd. Radiopharm.*, 2015, **58**(7), 308–312.

5 R. Roskoski, Sunitinib: A VEGF and PDGF receptor protein kinase and angiogenesis inhibitor, *Biochem. Biophys. Res. Commun.*, 2007, **356**(2), 323–328.

6 M. Sathish, A. P. Sakla, F. M. Nachtigall, L. S. Santos and N. Shankaraiah, TCCA-mediated oxidative rearrangement of tetrahydro-β-carbolines: facile access to spirooxindoles and the total synthesis of (±)-coerulescine and (±)-horsfi-line, *RSC Adv.*, 2021, **11**(27), 16537–16546.

7 M. Alamgir, P. S. R. Mitchell, P. K. Bowyer, N. Kumar and D. S. Black, Synthesis of 4,7-indoloquinones from indole-7-carbaldehydes by Dakin oxidation, *Tetrahedron*, 2008, **64**(30), 7136–7142.

8 X. Zhang and C. S. Foote, Dimethyldioxirane oxidation of indole derivatives. Formation of novel indole-2,3-epoxides and a versatile synthetic route to indolinones and indo-lines, *J. Am. Chem. Soc.*, 1993, **115**(19), 8867–8868.

9 J. Wang, Y. Chen, W. Du, N. Chen, K. Fu, Q. He and L. Shao, Green oxidative rearrangement of indoles using halide catalyst and hydrogen peroxide, *Tetrahedron*, 2022, **127**, 133101.

10 J. Xu, L. Liang, H. Zheng, Y. R. Chi and R. Tong, Green oxi-dation of indoles using halide catalysis, *Nat. Commun.*, 2019, **10**(1), 4754.

11 D. Decembrino and D. Cannella, The thin line between monooxygenases and peroxygenases. P450s, UPOs, MMOs, and LPMOs: A brick to bridge fields of expertise, *Biotechnol. Adv.*, 2024, **72**, 108321.

12 M. Hobisch, D. Holtmann, P. Gomez de Santos, M. Alcalde, F. Hollmann and S. Kara, Recent developments in the use of peroxygenases – Exploring their high potential in selec-tive oxyfunctionalisations, *Biotechnol. Adv.*, 2021, **51**, 107615.

13 J. Aburto, J. Correa-Basurto and E. Torres, Atypical kinetic behavior of chloroperoxidase-mediated oxidative halogena-tion of polycyclic aromatic hydrocarbons, *Arch. Biochem. Biophys.*, 2008, **480**(1), 33–40.

14 M. Sundaramoorthy, J. Terner and T. L. Poulos, Stereochemistry of the chloroperoxidase active site: crystal-lographic and molecular-modeling studies, *Chem. Biol.*, 1998, **5**(9), 461–473.

15 V. Yazbik and M. Ansorge-Schumacher, Fast and efficient purification of chloroperoxidase from C. fumago, *Process Biochem.*, 2010, **45**(2), 279–283.

16 G. Masdeu, M. Pérez-Trujillo, J. López-Santín and G. Álvaro, Chloroperoxidase-catalyzed amino alcohol oxidation: Substrate specificity and novel strategy for the synthesis of N-Cbz-3-aminopropanal, *Process Biochem.*, 2016, **51**(9), 1204–1211.

17 A. Zaks and D. R. Dodds, Chloroperoxidase-catalyzed asymmetric oxidations: substrate specificity and mechanistic study, *J. Am. Chem. Soc.*, 1995, **117**(42), 10419–10424.

18 M. P. J. van Deurzen, F. van Rantwijk and R. A. Sheldon, Selective oxidations catalyzed by peroxidases, *Tetrahedron*, 1997, **53**(39), 13183–13220.

19 L. P. Hager, F. J. Lakner and A. Basavapathruni, Chiral synthons via chloroperoxidase catalysis, *J. Mol. Catal. B: Enzym.*, 1998, **5**(1), 95–101.

20 F. Gao, L. Wang, Y. Liu, S. Wang, Y. Jiang, M. Hu, S. Li and Q. Zhai, Enzymatic synthesis of (R)-modafinil by chloroperoxidase-catalyzed enantioselective sulfoxidation of 2-(diphenylmethylthio) acetamide, *Biochem. Eng. J.*, 2015, **93**, 243–249.

21 M. P. J. van Deurzen, F. van Rantwijk and R. A. Sheldon, Chloroperoxidase-Catalyzed Oxidation of 5-Hydroxymethylfurfural, *J. Carbohydr. Chem.*, 1997, **16**(3), 299–309.

22 J. L. García-Zamora, K. León-Aguirre, R. Quiroz-Morales, R. Parra-Saldívar, M. B. Gómez-Patiño, D. Arrieta-Baez, G. Rebollar-Pérez and E. Torres, Chloroperoxidase-Mediated Halogenation of Selected Pharmaceutical Micropollutants, *Catalysts*, 2018, **8**(1), 32.

23 M. A. Pickard, T. A. Kadima and R. D. Carmichael, Chloroperoxidase, a peroxidase with potential, *J. Ind. Microbiol.*, 1991, **7**(4), 235–241.

24 D. Jung, C. Streb and M. Hartmann, Oxidation of indole using chloroperoxidase and glucose oxidase immobilized on SBA-15 as tandem biocatalyst, *Microporous Mesoporous Mater.*, 2008, **113**(1), 523–529.

25 R. Zhang, Q. He, D. Chatfield and X. Wang, Paramagnetic Nuclear Magnetic Resonance Relaxation and Molecular Mechanics Studies of the Chloroperoxidase–Indole Complex: Insights into the Mechanism of Chloroperoxidase-Catalyzed Regioselective Oxidation of Indole, *Biochemistry*, 2013, **52**(21), 3688–3701.

26 M. P. J. van Deurzen, F. van Rantwijk and R. A. Sheldon, Synthesis of substituted oxindoles by chloroperoxidase catalyzed oxidation of indoles, *J. Mol. Catal. B: Enzym.*, 1996, **2**(1), 33–42.

27 M. P. J. van Deurzen, I. J. Remkes, F. van Rantwijk and R. A. Sheldon, Chloroperoxidase catalyzed oxidations in t-butyl alcohol/water mixtures, *J. Mol. Catal. A: Chem.*, 1997, **117**(1), 329–337.

28 K. Seelbach, M. P. J. van Deurzen, F. van Rantwijk, R. A. Sheldon and U. Kragl, Improvement of the total turnover number and space-time yield for chloroperoxidase catalyzed oxidation, *Biotechnol. Bioeng.*, 1997, **55**(2), 283–288.

29 S. Peter, M. Kinne, R. Ullrich, G. Kayser and M. Hofrichter, Epoxidation of linear, branched and cyclic alkenes catalyzed by unspecific peroxygenase, *Enzyme Microb. Technol.*, 2013, **52**(6), 370–376.

30 S. Peter, A. Karich, R. Ullrich, G. Gröbe, K. Scheibner and M. Hofrichter, Enzymatic one-pot conversion of cyclohexane into cyclohexanone: Comparison of four fungal peroxygenases, *J. Mol. Catal. B: Enzym.*, 2014, **103**, 47–51.

31 D. I. Perez, M. M. Grau, I. W. C. E. Arends and F. Hollmann, Visible light-driven and chloroperoxidase-catalyzed oxygenation reactions, *Chem. Commun.*, 2009, (44), 6848–6850.

32 J. M. Campos-Martin, G. Blanco-Brieva and J. L. G. Fierro, Hydrogen Peroxide Synthesis: An Outlook beyond the Anthraquinone Process, *Angew. Chem., Int. Ed.*, 2006, **45**(42), 6962–6984.

33 H. L. Wapshott-Stehli and A. M. Grunden, In situ H_2O_2 generation methods in the context of enzyme biocatalysis, *Enzyme Microb. Technol.*, 2021, **145**, 109744.

34 F. Tieves, S. J.-P. Willot, M. M. C. H. van Schie, M. C. R. Rauch, S. H. H. Younes, W. Zhang, J. Dong, P. Gomez de Santos, J. M. Robbins, B. Bommarius, *et al.*, Formate Oxidase (FOx) from Aspergillus oryzae: One Catalyst Enables Diverse H_2O_2-Dependent Biocatalytic Oxidation Reactions, *Angew. Chem., Int. Ed.*, 2019, **58**(23), 7873–7877.

35 Y. Ma, Y. Li, S. Ali, P. Li, W. Zhang, M. C. R. Rauch, S. J.-P. Willot, D. Ribitsch, Y. H. Choi, M. Alcalde, *et al.*, Natural Deep Eutectic Solvents as Performance Additives for Peroxygenase Catalysis, *ChemCatChem*, 2020, **12**(4), 989–994.

36 W. Zhang, B. O. Burek, E. Fernández-Fueyo, M. Alcalde, J. Z. Bloh and F. Hollmann, Selective Activation of C−H Bonds in a Cascade Process Combining Photochemistry and Biocatalysis, *Angew. Chem., Int. Ed.*, 2017, **56**(48), 15451–15455.

37 D. Holtmann, T. Krieg, L. Getrey and J. Schrader, Electroenzymatic process to overcome enzyme instabilities, *Catal. Commun.*, 2014, **51**, 82–85.

38 S. J. Freakley, S. Kochius, J. van Marwijk, C. Fenner, R. J. Lewis, K. Baldenius, S. S. Marais, D. J. Opperman, S. T. L. Harrison, M. Alcalde, *et al.*, A chemo-enzymatic oxidation cascade to activate C–H bonds with in situ generated H_2O_2, *Nat. Commun.*, 2019, **10**(1), 4178.

39 J. Brehm, R. J. Lewis, T. Richards, T. Qin, D. J. Morgan, T. E. Davies, L. Chen, X. Liu and G. J. Hutchings, Enhancing the Chemo-Enzymatic One-Pot Oxidation of Cyclohexane via In Situ H_2O_2 Production over Supported Pd-Based Catalysts, *ACS Catal.*, 2022, 11776–11789.

40 A. Stenner, R. J. Lewis, J. Brehm, T. Qin, Á. López-Martín, D. J. Morgan, T. E. Davies, L. Chen, X. Liu and G. J. Hutchings, Chemo-Enzymatic One-Pot Oxidation of Cyclohexane via *in situ* H_2O_2 Production over Supported AuPdPt Catalysts, *ChemCatChem*, 2023, **15**(10), e202300162.

41 A. Santos, R. J. Lewis, G. Malta, A. G. R. Howe, D. J. Morgan, E. Hampton, P. Gaskin and G. J. Hutchings,

Direct Synthesis of Hydrogen Peroxide over Au–Pd Supported Nanoparticles under Ambient Conditions, *Ind. Eng. Chem. Res.*, 2019, **58**(28), 12623–12631.

42 D. A. Crole, S. J. Freakley, J. K. Edwards and G. J. Hutchings, Direct synthesis of hydrogen peroxide in water at ambient temperature, *Proc. R. Soc. London, Ser. A*, 2016, **472**(2190), 20160156.

43 X. Gong, R. J. Lewis, S. Zhou, D. J. Morgan, T. E. Davies, X. Liu, C. J. Kiely, B. Zong and G. J. Hutchings, Enhanced catalyst selectivity in the direct synthesis of H_2O_2 through Pt incorporation into TiO2 supported AuPd catalysts, *Catal. Sci. Technol.*, 2020, **10**(14), 4635–4644.

44 J. Jeon and S. J. Kim, Recent Progress in Hydrogen Flammability Prediction for the Safe Energy Systems, *Energies*, 2020, **13**, 6263.

45 L. P. Hager, D. R. Morris, F. S. Brown and H. Eberwein, Chloroperoxidase: II. UTILIZATION OF HALOGEN ANIONS, *J. Biol. Chem.*, 1966, **241**(8), 1769–1777.

46 N. E. Ntainjua, J. K. Edwards, A. F. Carley, J. A. Lopez-Sanchez, J. A. Moulijn, A. A. Herzing, C. J. Kiely and G. J. Hutchings, The role of the support in achieving high selectivity in the direct formation of hydrogen peroxide, *Green Chem.*, 2008, **10**(11), 1162–1169.

47 Y. Zhang, Z. Lyu, Z. Chen, S. Zhu, Y. Shi, R. Chen, M. Xie, Y. Yao, M. Chi, M. Shao, *et al.*, Maximizing the Catalytic Performance of Pd@AuxPd1− Nanocubes in H_2O_2 Production by Reducing Shell Thickness to Increase Compositional Stability, *Angew. Chem., Int. Ed.*, 2021, **60**(36), 19643–19647.

48 T. Richards, J. H. Harrhy, R. J. Lewis, A. G. R. Howe, G. M. Suldecki, A. Folli, D. J. Morgan, T. E. Davies, E. J. Loveridge, D. A. Crole, *et al.*, A residue-free approach to water disinfection using catalytic in situ generation of reactive oxygen species, *Nat. Catal.*, 2021, **4**(7), 575–585.

49 D. W. Flaherty, Direct Synthesis of H_2O_2 from H2 and O2 on Pd Catalysts: Current Understanding, Outstanding Questions, and Research Needs, *ACS Catal.*, 2018, **8**(2), 1520–1527.

50 N. M. Wilson, P. Priyadarshini, S. Kunz and D. W. Flaherty, Direct synthesis of H_2O_2 on Pd and AuxPd1 clusters: Understanding the effects of alloying Pd with Au, *J. Catal.*, 2018, **357**, 163–175.

51 V. R. Choudhary, A. G. Gaikwad and S. D. Sansare, Activation of Supported Pd Metal Catalysts for Selective Oxidation of Hydrogen to Hydrogen Peroxide, *Catal. Lett.*, 2002, **83**(3), 235–239.

52 A. G. Gaikwad, S. D. Sansare and V. R. Choudhary, Direct oxidation of hydrogen to hydrogen peroxide over Pd-containing fluorinated or sulfated Al_2O_3, ZrO2, CeO_2, ThO2, Y2O3 and Ga2O3 catalysts in stirred slurry reactor at ambient conditions, *J. Mol. Catal. A: Chem.*, 2002, **181**(1), 143–149.

53 G. Blanco-Brieva, E. Cano-Serrano, J. M. Campos-Martin and J. L. G. Fierro, Direct synthesis of hydrogen peroxide solution with palladium-loaded sulfonic acid polystyrene resins, *Chem. Commun.*, 2004, **10**, 1184–1185.

54 D. I. Enache, J. K. Edwards, P. Landon, B. Solsona-Espriu, A. F. Carley, A. A. Herzing, M. Watanabe, C. J. Kiely, D. W. Knight and G. J. Hutchings, Solvent-Free Oxidation of Primary Alcohols to Aldehydes Using Au-Pd/TiO_2 Catalysts, *Science*, 2006, **311**(5759), 362–365.

55 J.-B. Park and D. S. Clark, Deactivation mechanisms of chloroperoxidase during biotransformations, *Biotechnol. Bioeng.*, 2006, **93**(6), 1190–1195.

56 J.-B. Park and D. S. Clark, New reaction system for hydrocarbon oxidation by chloroperoxidase, *Biotechnol. Bioeng.*, 2006, **94**(1), 189–192.

57 N. Tanaka, C. Ikeda, K. Kanaori, K. Hiraga, T. Konno and S. Kunugi, Pressure effect on the conformational fluctuation of apomyoglobin in the native state, *Biochemistry*, 2000, **39**(39), 12063–12068.

58 J. Saad-Nehme, J. L. Silva and J. R. Meyer-Fernandes, Osmolytes protect mitochondrial F0F1-ATPase complex against pressure inactivation, *Biochim. Biophys. Acta*, 2001, **1546**(1), 164–170.

59 P. Masson, C. Cléry, P. Guerra, A. Redslob, C. Albaret and P. L. Fortier, Hydration change during the aging of phosphorylated human butyrylcholinesterase: Importance of residues aspartate-70 and glutamate-197 in the water network as probed by hydrostatic and osmotic pressures, *Biochem. J.*, 1999, **343**(2), 361–369.

60 M. Ayala, C. V. Batista and R. Vazquez-Duhalt, Heme destruction, the main molecular event during the peroxide-mediated inactivation of chloroperoxidase from Caldariomyces fumago, *J. Biol. Inorg. Chem.*, 2011, **16**(1), 63–68.

61 B. Valderrama, M. Ayala and R. Vazquez-Duhalt, Suicide Inactivation of Peroxidases and the Challenge of Engineering More Robust Enzymes, *Chem. Biol.*, 2002, **9**(5), 555–565.

62 F. A. Muñoz-Guerrero, S. Águila, R. Vazquez-Duhalt, C. C. Torres, C. H. Campos and J. B. Alderete, Biocatalytic Performance of Chloroperoxidase from Caldariomyces fumago Immobilized onto TiO2 Based Supports, *Top. Catal.*, 2016, **59**(2), 387–393.

63 T. Krieg, S. Hüttmann, K.-M. Mangold, J. Schrader and D. Holtmann, Gas diffusion electrode as novel reaction system for an electro-enzymatic process with chloroperoxidase, *Green Chem.*, 2011, **13**(10), 2686–2689.

64 F. van de Velde, N. D. Lourenço, M. Bakker, F. van Rantwijk and R. A. Sheldon, Improved operational stability of peroxidases by coimmobilization with glucose oxidase, *Biotechnol. Bioeng.*, 2000, **69**(3), 286–291.

65 P. Molina-Espeja, E. Garcia-Ruiz, D. Gonzalez-Perez, R. Ullrich, M. Hofrichter and M. Alcalde, Directed Evolution of Unspecific Peroxygenase from Agrocybe aegerita, *Appl. Environ. Microbiol.*, 2014, **80**(11), 3496–3507.

66 J. Zdarta, A. S. Meyer, T. Jesionowski and M. Pinelo, Developments in support materials for immobilization of oxidoreductases: A comprehensive review, *Adv. Colloid Interface Sci.*, 2018, **258**, 1–20.

67 G. Espina, J. Atalah and J. M. Blamey, Extremophilic Oxidoreductases for the Industry: Five Successful Examples With Promising Projections, *Front. Bioeng. Biotechnol.*, 2021, **9**, 710035.

68 A. Brandolese, D. H. Lamparelli, M. A. Pericàs and A. W. Kleij, Synthesis of Biorenewable Terpene Monomers Using Enzymatic Epoxidation under Heterogeneous Batch and Continuous Flow Conditions, *ACS Sustainable Chem. Eng.*, 2023, **11**(12), 4885–4893.

69 A. Basso and S. Serban, Industrial applications of immobilized enzymes—A review, *Mol. Catal.*, 2019, **479**, 110607.

70 H. Gröger, F. Gallou, H. Bruce and B. H. Lipshutz, Where Chemocatalysis Meets Biocatalysis: In water, *Chem. Rev.*, 2023, **123**(9), 5262–5296.